A trigeneration system based on polymer electrolyte fuel cell and desiccant wheel – Part B: Overall system design and energy performance analysis

M. Intini *, S. De Antonellis, C.M. Joppolo, A. Casalegno

Department of Energy, Politecnico di Milano, via Lambruschini 4, 20156 Milan, Italy

Received 28 July 2015
Accepted 3 October 2015
Available online 26 October 2015

1. Introduction

Combined heating, cooling and power unit based on fuel cells are of great interest due to potential increase in overall efficiency, reduction in primary energy consumption and near-zero emissions.

At present many research works deal with design and feasibility of trigenerative power plants. Kavvadias et al. [1], Balli et al. [2,3] and Zhao et al. [4] focused on trigenerative applications driven by internal combustion engines, Wang et al. [5] optimized an organic Rankine cycle-based CHCP system driven by solar energy while Al-Sulaiman et al. [6] compared electrical efficiency and cost rate of CHCP systems based on SOFC units, biomass and solar energy. Particular attention is given to small scale systems for distributed units [7]; domestic scale trigeneration systems have a great potential but profitability [8] and performance of heat driven devices [9] are still key issues to cope with. Several research works deal with trigeneration based on fuel cells: Gabbar et al. [10] focused on a fuel cell system for energy conservation in a commercial building. The use of high temperature exhaust gas from SOFC has been widely discussed by Choudhury et al. [11]. Zink et al. [12] investigated the use of SOFC to provide heating, cooling and domestic hot water for buildings. Chen and Ni [13], Ranjbar et al. [14] and Fong and Lee [15] analyzed systems based on SOFC and absorption chiller, Al-Sulaiman et al. [16] evaluated energy performance of a system based on SOFC, organic Rankine cycle and absorption chiller and Tse et al. [17] investigated a SOFC hybrid trigenerative system for marine applications.

The use of PEMFC system is largely investigated in cogenerative arrangement such as households [18] or commercial greenhouses [19]. High temperature PEMFC for micro-cogeneration generally

* Corresponding author. Tel.: +39 02 2399 3874.
E-mail address: manuel.intini@polimi.it (M. Intini).

Nomenclature

Acronyms

CC	cooling coil
CR	capacity ratio
DEC	Desiccant Evaporative Cooling
DW	desiccant wheel
EC	Evaporative Cooler
EER	Energy Efficiency Ratio
F	Fan
HTHX	High Temperature Heat Exchanger
HTS	High Temperature heat Sink
HTT	High Temperature heat Tank
LTHX	Low Temperature Heat Exchanger
HTS	High Temperature heat Sink
HTT	High Temperature heat Tank
HW	heat wheel
MSBT	minimum stand-by time
PEC	Primary Energy Consumption
PEM	Polymer Electrolyte Membrane
PEMFC	Polymer Electrolyte Membrane Fuel Cell
PES	primary energy saving
PLR	part load ratio
TPES	Trigeneration Primary Energy Saving

Symbols

C	cooling energy [MW h]
C_u	sensible and latent useful cooling energy [MW h]
$\dot{C}$	cooling capacity [kW]
F	fuel consumption [MW h]
$\dot{F}$	fuel consumption rate [kW]
Q	thermal energy [MW h]
Q_u	sensible and latent useful heating energy [MW h]
$\dot{Q}$	heating capacity [kW]
T	temperature [°C]
x	humidity ratio [g/kg]
U	overall heat transfer coefficient [W/m^2/K]
v	velocity [m/s]
V	volumetric flow rate [m^3/h]
W	electrical energy [MW h]
W_u	useful electrical energy [MW h]
$\dot{W}$	electrical power [kW]

Subscripts

60%	at 60% of maximum load
100%	at full load
a	air
AHU	air handling unit
b	boiler
c	vapor compression chiller
el	electrical
ext	external
F	fan
HS	heat sinks
in	inlet
j	generic *j* component
loss	heat loss
LTS	low temperature heat sink
LTT	low temperature heat tank
max	maximum
min	minimum
out	outlet
P	pump
peak	peak load condition
ref	reference system
rb	reference building
SB	stand-by
ST	storage tanks
tri	trigenerative system
tot	total
w	water

Superscript

i	time step

Greek letters

α	air conditioning loads scaling factor
ΔP	pressure drop
ΔW	difference in electrical energy consumption
η	efficiency

leads to higher primary energy saving due to a better electrical efficiency [20,21]. Only a small number of works deal with a trigenerative configuration integrating absorption chillers [22,23], mainly due to the low fuel cell operating temperature which limits the performance of the heat driven cooling process.

In case of trigenerative systems driven by a low temperature heat source ($T < 70$ °C), desiccant wheel-based dehumidification units integrated with vapor compression cooling devices represent a suitable technology [24]. Other thermally driven cooling devices, such as adsorption or absorption chillers, suffer from poor energy efficiency ratio, which is limited to 0.5 in the best working conditions [25,26]. On the other hand it is shown that desiccant wheel-based cooling can actually save primary energy compared to the reference technology, especially if coupled with cogenerators [24,27,28] or even gas heaters [29]; in addition, indoor air quality can benefit from sorption wheels [30]. However energy savings strongly depend on boundary conditions, such as air temperature and humidity, sensible and latent loads.

As reported in part A [41] of this work, low temperature PEMFC systems are quite a mature technology in terms of yearly operating hours and potential applications. In the present paper a trigeneration system integrating a low temperature PEM fuel cell and a desiccant wheel based air handling unit is designed and analyzed. Technical constraints, specifications of real systems and actual performance of each device at full and part load are precisely taken into account. According to the foregoing literature review, such a system has not been investigated in spite of possible energy savings compared to the conventional technology.

Energy simulations are carried out for a trigenerative plant coupled with an office building and performance are assessed on yearly basis in terms of TPES (Trigeneration Primary Energy Saving) [31]. The optimal system configuration is identified and the effect of climate conditions is evaluated. Finally the effects of PEMFC system improvements are analyzed and the increase in the primary energy saving is evaluated.

2. Adopted performance index of the trigenerative system

In the present work TPES (Trigeneration Primary Energy Saving) index [31] is used to evaluate the potential benefits of the trigenerative system. According to Fig. 1, the control volumes include:

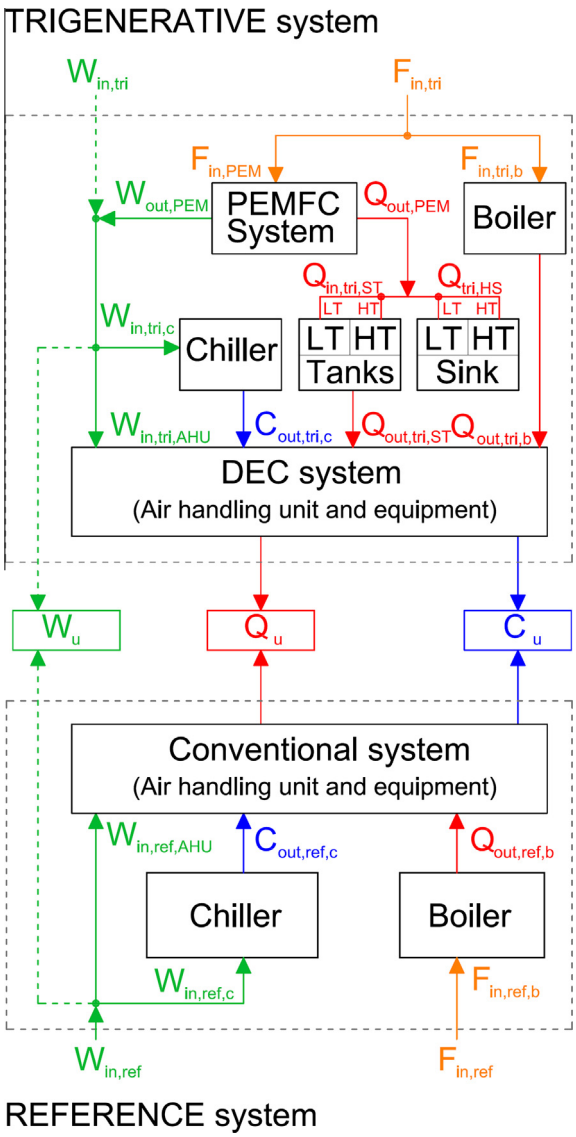

Fig. 1. A schematic of the trigeneration system and of the standard reference system.

- The trigenerative system, composed of a PEMFC system, an auxiliary boiler, heat storages, a vapor compression chiller and a DEC air handling unit.
- The reference system, composed of a boiler, a vapor compression chiller and a conventional air handling unit.

The TPES index assumes the following form (Eqs. (1) and (2)):

$$\mathrm{TPES} = 1 - \frac{\mathrm{PEC}_{tri}}{\mathrm{PEC}_{ref}} \tag{1}$$

$$\mathrm{TPES} = 1 - \frac{\sum_i \left(F^i_{in,tri} + W^i_{in,tri}/\eta_{el,ref}\right)}{\sum_i \left(F^i_{in,ref} + W^i_{in,ref}/\eta_{el,ref}\right)} \tag{2}$$

Since the trigenerative system is designed to meet thermal loads, which are extremely variable over the year, the amount of cogenerated electricity is not constant and may not be enough to balance air conditioning electrical consumptions, which include the energy required by the air handling unit and the vapor compression chiller. Referring to Fig. 1, whether the cogenerated electricity $W_{out,PEM}$ is higher than electrical consumption of the chiller $W_{in,tri,c}$ and of the air handling unit $W_{in,tri,AHU}$, the surplus $W_u = (W_{out,PEM} - W_{in,tri,c} - W_{in,tri,AHU})$ is a useful output for on-site consumption. Instead, if $W_{out,PEM}$ is not sufficient to meet electrical loads, integrating electric power $W_{in,tri}$ is drawn from the national grid. For the reference system natural gas $F_{in,ref}$ and electrical energy $W_{in,ref}$ are used to drive a standard boiler, a vapor compression chiller and a conventional air handling unit. If the trigeneration system supplies a useful electrical output W_u, the standard system draws additional electrical energy from the national electric grid.

The reference value of electric efficiency in separated power production is calculated according to the Italian legislation, as shown by Campanari et al. [32]. Assuming that the electricity generated by the system is fully consumed onsite, the resulting adopted $\eta_{el,ref}$ is equal to 45.15%.

Eqs. (1) and (2) are based on annual or seasonal basis, since air conditioning systems can vary significantly over the entire year and the evaluation of TPES only in design conditions would lead to a misleading analysis.

3. Systems description, assumptions and operation strategy

3.1. Introduction

In this work performance of the proposed trigenerative system is evaluated and compared to the reference technology. In both configurations an all-air system is considered: both building sensible and latent loads are balanced exclusively through appropriate air treatments in the air handling unit. Simplified schemes of the reference and trigenerative systems are reported respectively in Figs. 2 and 3, while a detailed description of each component is described in Section 4.

The systems operate at constant air flow rate, which is assumed equal to the fresh air stream that should be supplied to the building. Supply air temperature and humidity ratio are calculated on hourly basis to meet sensible and latent loads.

3.2. Reference system

The reference system is based on a standard air handling unit in a double flow arrangement, namely supply flow and exhaust flow. As shown in Fig. 2, the air handling unit is equipped with a sensible heat wheel (HW), a heating coil (HC), a cooling/heating coil (CCA), two evaporative coolers (ECA and ECB) and two fans (FA, FB). Supply flow is either heated up in winter time or cooled down in

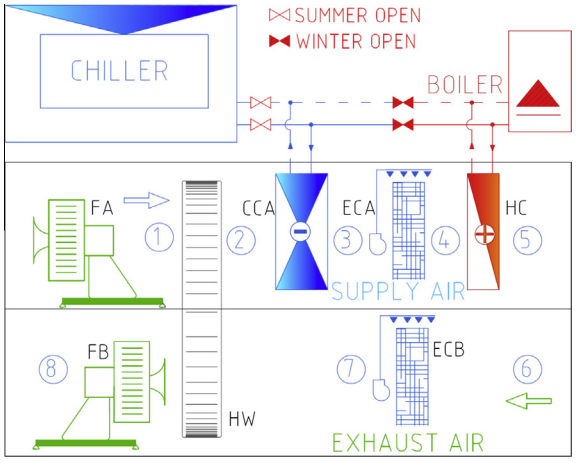

Fig. 2. Scheme of the reference system.

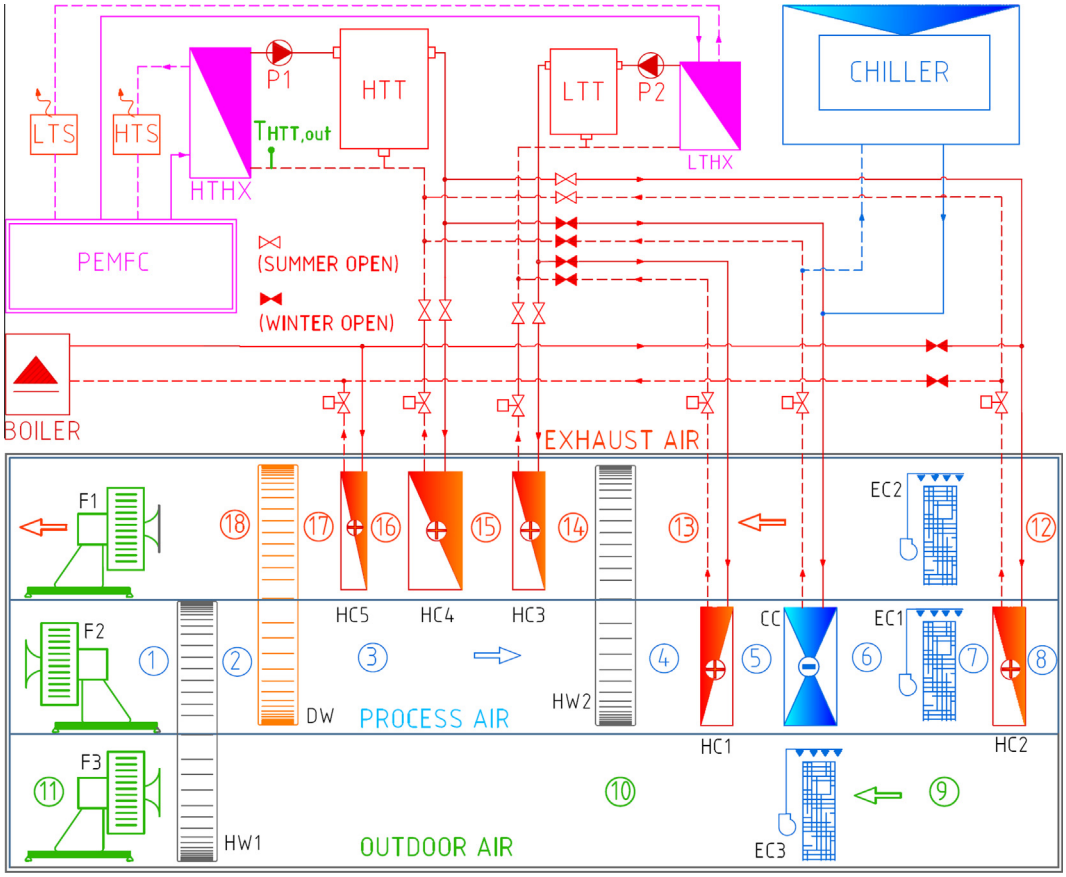

Fig. 3. A schematic of the DEC air handling unit coupled with PEMFC.

summer time by the exhaust flow across HW (1–2). Than it is either heated in winter or cooled and dehumidified in summer through CCA (2–3). Afterward it is humidified through ECA (3–4) in winter (no process occurs in summer) and finally temperature is adjusted by HC (5–6) both in winter or summer time. Exhaust air is heated or cooled across HW (7–8) and, in summer time, it is cooled through the humidifier ECB (6–7).

In winter period supply air stream is heated across the heat wheel and the two heating coils and it is humidified through the evaporative cooler. The exhaust air stream leaving the building is cooled down across the heat wheel. In summer time, process air is cooled across the heat wheel, than it is dehumidified across a cooling coil down to the required supply humidity ratio. The post-heating coil adjusts the air flow temperature if necessary.

Hot water is provided by a standard boiler while chilled water for dehumidification and cooling is provided by an air cooled vapor compression chiller. Heat transfer between piping and surrounding is neglected.

The electric power consumption of the reference system at each time step i is (Eq. (3)):

$$W^i_{in,ref} = W^i_{in,ref,AHU} + W^i_{in,ref,c} + W^i_u = W^i_{in,ref,FA} + W^i_{in,ref,FB} + \frac{C^i_{out,ref,c}}{EER^i_c} + W^i_u \quad (3)$$

where $C_{out,ref,c}$ is equal to the load of cooling coil CCA and EER^i_c is the chiller energy efficiency ratio. W^i_u is the net power production of the proposed trigenerative system delivered to the building, which can be positive or equal to zero. This term is added to the electric power consumption of the reference system in order to make it comparable to the proposed trigenerative technology.

Fuel consumption is calculated through Eq. (4):

$$F^i_{in,ref} = F^i_{in,ref,b} = \frac{Q^i_{out,ref,b}}{\eta^i_{ref,b}} \quad (4)$$

where the heat released by the boiler is the total heat required by the two heating coils (CCA, HC):

$$Q^i_{out,ref,b} = Q^i_{CCA} + Q^i_{HC} \quad (5)$$

3.3. Proposed trigenerative system

The trigenerative unit consists of a PEMFC system and of a desiccant wheel air handling unit. Three main air flows can be distinguished: supply (or process) air flow, outdoor air flow and exhaust (or return) air flow. The air handling unit (Fig. 3) includes a desiccant wheel (DW), two heat wheels (HW1, HW2), five heating coils (HC1–HC5), a cooling/heating coil (CC), three evaporative coolers (EC1–EC3) and three fans (F1–F3).

In winter mode the air handling unit works similarly to the reference system: exhaust air stream from the building is used to preheat the supply air flow while outdoor air is not adopted. Therefore fan F3, evaporative coolers EC2 and EC3, heat wheel HW1, desiccant wheel DW and the three heating coils HC3–HC5 do not operate. Supply air stream flows through the heat wheel HW2, the heating coil HC1, CC and HC2 and the humidifier EC1 as described for the reference system.

In summer mode process air treatments are based on the open loop Pennington cycle [33] with the integration of a sensible cooling process to adjust supply air temperature. In this condition the heating coils HC1 and HC2 and the humidifier EC1 do not operate,

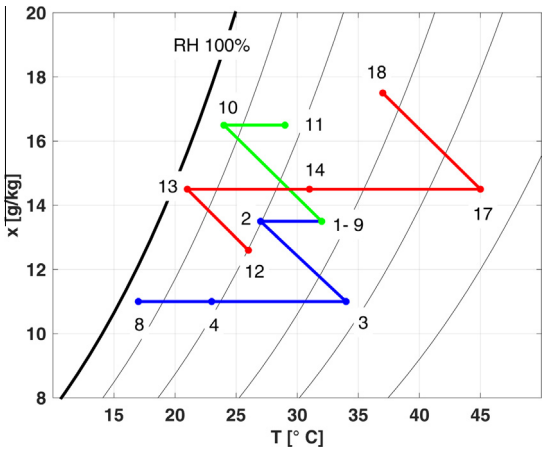

Fig. 4. A typical summer air flow treatment for hybrid DEC system.

while the coil CC is provided with chilled water to operate as sensible cooling component. As shown in Fig. 4, process air stream at external conditions is first cooled down (1–2) through the heat wheel (HW1) by a secondary outdoor air stream (10–11) which is previously cooled through the direct evaporative cooler EC3 (9–10); than air flow is dehumidified (2–3) across a desiccant wheel DW, which is simultaneously regenerated by exhaust air (17–18) previously heated across coils HC3–HC5 (14–17). Then process air flow is cooled down in the heat wheel HW2 (3–4) by exhaust air flow (13–14) previously cooled through the evaporative humidifier EC2 (12–13). Finally the cooling coil CC adjusts the supply flow temperature if needed (4–8).

If dehumidification is not required, indirect evaporative cooler and desiccant wheel are not active, the incoming supply air stream at outdoor conditions flows directly to the heat wheel HW2 and then temperature is adjusted across the cooling coil CC.

As shown in part A of this work, at PEMFC full load almost 22% of cogeneration heat is released through a low temperature ($T \approx 45$ °C) heat exchanger (LTHX) while the remaining 78% is available through the high temperature ($T \approx 65$ °C) heat exchanger (HTHX). Each of them delivers heat to a water loop connected to the respective low temperature and high temperature tanks (LTT and HTT). Low temperature tank provides hot water to HC1 in winter time and to HC3 in summer time while high temperature storage supplies hot water respectively to CC and HC4. A backup boiler supplies hot water to HC2 during winter and HC5 during summer.

Additional heat sinks LTS and HTS are installed in each water loop to provide the necessary thermal dissipation when return water from heat tanks is too high and not compatible with PEMFC system constraints. Although heat sinks are necessary to cope with PEMFC poor flexibility, they can be a main cause of primary energy waste, since thermal output may be not exploited completely.

The present PEMFC system is manufactured by ICI Caldaie, which has provided additional technical details through a personal communication. Such details are provided throughout the current work and their impact on system performance is discussed in the sensitivity analysis in Section 5.4. PEMFC system can operate at part load conditions between 60% and 100% of the electric power output or in stand-by mode, with only limited natural gas combustion to keep reformer temperature above a required level. Proper control logic must be used to set PEMFC unit part load operating condition in relation to the thermal load. This is essential no to waste significant amount of thermal energy across the heat sinks.

Since most of cogeneration heat is released through the high temperature heat exchanger, return water temperature from HTT is used as feedback quantity to set the PEMFC system at part load condition or in stand-by mode. More precisely, referring to Fig. 3, the adopted operating strategy acts as follows:

- If $T_{HTT,out} > T_{HTT,out,max}$, PEMFC is switched to stand-by mode.
- If $T_{HTT,out} < T_{HTT,out,min}$, PEMFC works at full load.
- If $T_{HTT,out,min} < T_{HTT,out} < T_{HTT,out,max}$, the PEMFC system power capacity is controlled in each time step i through the following relation:

$$F^i_{in,tri,PEM} = F^i_{in,tri,PEM,100\%} - \frac{T^i_{HTT,out} - T^i_{HTT,out,min}}{T^i_{HTT,out,max} - T^i_{HTT,out,min}} \left(F^i_{in,tri,PEM,100\%} - F^i_{in,tri,PEM,60\%}\right) \tag{6}$$

Based on preliminary analysis, $T_{HTT,out,max} = 55$ °C and $T_{HTT,out,min} = 45$ °C turn out to be optimal values to maximize PEMFC heating output with minimal heat rejection. According to manufacturer technical specifications, the system partialization is achieved through fixed reduction step of 10% of the full load heating capacity and it is assumed that the PEMFC unit may complete such a step in one hour. Instead no similar constraints are considered for increasing heat load.

Finally, the heat released to the low temperature loop is not controlled: if tank temperature increases too much, heat released by the PEMFC system is dissipated through the heat sink.

According to Figs. 1 and 2, at each time step i, if the power production of the trigenerative system is higher than self-consumption of the system, Eq. (7) is applied:

$$\begin{cases} W^i_{in,tri} = 0 \\ W^i_u = W^i_{out,PEM} - W^i_{in,tri,c} - W^i_{in,tri,AHU} \end{cases} \tag{7}$$

Instead, if $W^i_{out,PEM} < W^i_{in,tri,c} + W^i_{in,tri,AHU}$, W_u and $W_{in,tri}$ are calculated through Eq. (8):

$$\begin{cases} W^i_u = 0 \\ W^i_{in,tri} = W^i_{in,tri,c} + W^i_{in,tri,AHU} - W^i_{out,PEM} \end{cases} \tag{8}$$

Electric power consumption of chiller and air handling unit equipment are calculated according to Eqs. (9) and (10):

$$W^i_{in,tri,c} = \frac{C^i_{out,tri,c}}{\mathrm{EER}^i_{tri,c}} = \frac{C^i_{tri,CC1}}{\mathrm{EER}^i_{tri,c}} \tag{9}$$

$$W^i_{in,tri,AHU} = \sum_{j=1}^{3} W^i_{in,tri,Fj} + \sum_{j=1}^{2} W^i_{in,tri,Pj} \tag{10}$$

Fuel consumption is:

$$F^i_{in,tri} = F^i_{in,tri,PEM} + F^i_{in,tri,b} = F^i_{in,tri,PEM} + \frac{Q^i_{out,tri,b}}{\eta^i_{tri,b}} \tag{11}$$

Heat released by the boiler is total heat required by the heating coils HC5 (in summer condition) and HC2 (in winter condition):

$$Q^i_{out,tri,b} = Q^i_{tri,HC2} + Q^i_{tri,HC5} \tag{12}$$

4. Components modeling

4.1. Introduction

Each component of the reference and of the trigenerative system is described in detail in the following sections.

4.2. PEMFC

The PEMFC system and its full load and part load performance are described in detail in part A of this work. Since the PEMFC cannot be switched off daily to ensure an adequate fuel processor lifetime, fuel consumption to keep the reformer at a proper temperature should be considered. The total amount of energy needed is referred to as stand-by (SB) energy consumption. This quantity has been determined according to the information provided by the manufacturer and it includes fuel consumption $\dot{F}_{in,PEM,SB} = 2$ kW and additional electric power $\dot{W}_{in,tri,SB} = 0.3$ kW for auxiliaries. A further technical constraint is the minimum stand-by time (MSBT), which is the minimum number of hours over which the PEMFC must be kept in stand-by mode before switching to operating mode. According to the personal communication of PEMFC manufacturer, MSBT has been kept equal to 3 h.

4.3. Boiler

In both reference and trigenerative configuration, it is simply assumed that modular boilers are installed in the system. Therefore in each time step boiler performance is calculated as follows:

- Between 10% and 100% of the heating capacity boilers operate at constant thermal efficiency $\eta_b^i = \eta_{b,100\%}$.
- Between 0% and 10% of the heating capacity the thermal efficiency η_b^i increases linearly between 0 and $\eta_{b,100\%}$.

4.4. Vapor compression chiller

In each time step i, the chiller energy efficiency ratio EER_c is calculated as function of outdoor air temperature T_{ext}, as water supply chilled water temperature $T_{out,c}$ and part load ratio PLR, that is the ratio of actual cooling load to maximum chiller cooling capacity $\dot{C}_{max,out,c}$ calculated at T_{ext} and $T_{out,c}$. Chiller operates at constant supply chilled water temperature, which is set equal to 7 °C. A preliminary analysis has shown that raising chilled water temperature would lead to very large cooling coils and, therefore, high pressure drop, which affects electrical consumption detrimentally. In this work air cooled vapor compression chillers based on a scroll compressors with R-410 refrigerant are adopted. Depending on maximum cooling load, a single compressor or a multi compressors chiller is considered. EER_c calculation is based on data provided by an industrial manufacturer [34].

4.5. Heat tanks and plate heat exchangers

The high and low temperature heat storages are modeled through a multi-node approach [35] in order to take into account water stratification. Therefore the tank is modeled as divided in several sections and energy balance is solved in each of them. A sub-time step of 5 s has been found to be a good value to assure solution independency of temporal discretization. Finally heat tanks are assumed to have a cylindrical shape, with an aspect ratio equal to 2.5, made of steel insulated with foam [36] ($U = 0.786$ W/m^2/K).

Plate heat exchangers LTHX and HTHX are simply modeled through a constant effectiveness approach, being effectiveness equal to 0.80 for both of them.

4.6. Air handling unit

Air handling unit heating and cooling coils are appropriately designed according to peak load in winter and summer time. Both air handling units have been designed with an average and constant air velocity of 1.5 m/s. Each component is described in detail in the following.

4.6.1. Heating and cooling coil

Finned-tube air to water heat exchanger have been adopted. A manufacturer software [37] has been used to design the coils in order to match the peak heating and cooling loads and to calculate air pressure drops.

At part load conditions, the sensible heat released by coil HC1, CC1, HC3 and HC4 of the trigenerative configuration is calculated assuming that each overall heat transfer coefficient is constant in order to find water return temperature to the tank. For all of the other coils, two way valves are assumed to modulate heat or cooling; the ratio of actual to maximum heating or cooling released is adopted to calculate boilers and chiller efficiency. Due to the limited PEMFC system supply temperatures and the necessity of a storage tank, heating coils are designed so that peak-load heating is provided with water supply temperature of 55 °C for CC and HC4 and 45 °C for HC1 and HC3, with design water temperature drop of 10 °C across all heat exchangers. The size of CC is increased to meet summer peak cooling load, if necessary. Chilled water is provided at constant temperature of 7 °C with 5 °C of temperature increase across the cooling coil.

4.6.2. Desiccant wheel

In this analysis, performance of a regular density silica gel desiccant wheel is calculated through a one dimensional gas side resistance model, based on heat and mass transfer equations, which is a good trade-off between solution accuracy and computational speed. The model calculates average outlet air temperature, air humidity and pressure drop of both process and regeneration air stream. A detailed description of the model, its validation and desiccant wheel properties are reported in literature [38]. Process area ratio is set equal to 0.5, while desiccant wheel size is chosen to keep air face velocity v equal to 2 m/s, which is a common design parameter. According to a preliminary analysis, 20 rev/h turned out to be a proper value of revolution speed to achieve optimal working condition.

4.6.3. Heat wheels

Heat wheel effectiveness and pressure drop are evaluated through a one dimensional lumped parameters model [39]. The wheel area has been divided into equal parts and the face velocity v and the revolution speed N have been kept constant respectively to 2 m/s and 15 rev/min.

4.6.4. Fans and pumps

The fan of each air handling unit is modeled through a constant efficiency approach and its electric power consumption is calculated in this way:

$$W_{in,Fj}^i = \frac{m_a^i \Delta P_a}{\rho_a \eta_{Fj}} \tag{13}$$

where ΔP_a is the air pressure drop in the air handling unit fed by the fan and η_{Fj} is its electric efficiency equal to 0.75. Pressure drop of air filters is assumed constant while the one of the remaining components is calculated according to the information provided in Section 4.6.

In the trigenerative system, pump energy consumption for water loops from PEMFC heat exchangers to storage tanks have been properly taken into account. The electricity consumption of each pump is calculated as follows:

$$W_{in,Pj}^i = \frac{m_w^i \Delta P_w}{\rho_w \eta_{Pj}} \tag{14}$$

where ΔP_w is the pressure drop across heat exchangers and coils of each water loop and η_{Pj} is the pump efficiency, assumed constant and equal to 0.76. Mass flow rates are equal to 0.305 and 1.279 kg/s for low and high temperature water loops respectively, with a total pressure drop of 75 kPa for both loops.

Energy consumption of chiller and boiler pumps of the reference and the trigenerative system are similar and are assumed to be small compared to the electricity use of other equipment, therefore they have been neglected.

4.7. Building loads

4.7.1. Reference buildings

The reference building adopted in the energy simulations consists of a lecture room [40] with high level of occupancy (2 m^2 per person). The office is rectangular (12 × 18 m) with a total floor area of 216 m^2. Total glazed area is 63 m^2, which is roughly the 50% of total wall surface area. Minimal fresh air is set to 36 m^3/h per person which leads to a volumetric air flow rate $V_{a,rb}$ = 4000 mc/h (1.33 kg/s assuming a reference air density equal to 1.2 kg/m^3). Infiltration rate is set equal to 20% of office volume per hour, which is a realistic value for new building leakage envelope. Regarding other sources of sensible loads, only artificial lightning is taken into account. Sensible and latent heating and cooling loads $\dot{Q}_u$ and $\dot{C}_u$ are calculated with TRNSYS™ software on hourly basis. At a second stage, the power $\dot{Q}_{rb,out,ref}$, $\dot{Q}_{rb,out,tri}$, $\dot{C}_{rb,out,ref}$ and $\dot{C}_{rb,out,tri}$ required respectively by the heating and cooling coils of the AHU of reference and trigenerative system, are determined. Resulting values in peak conditions (the highest value in the whole year) are $\dot{Q}_{peak,rb,out,ref} = \dot{Q}_{peak,rb,out,tri}$ 42.94 kW, $\dot{C}_{peak,rb,out,ref}$ = 21.72 kW and $\dot{C}_{peak,rb,out,tri}$ = 12.34 kW. $\dot{Q}_{peak,rb,out}$ is equal for both the reference and trigenerative system because the peak condition occurs in winter time, when the air processes are the same, as shown in Sections 3.2 and 3.3.

4.7.2. Scaled building loads

Since PEMFC system cannot meet building thermal loads instantaneously, thermal storages and backup heating devices are necessary to operate continuously with minimal interruption. Hence the PEMFC system heating capacity can be lower than the one required by heating coils in peak conditions; indeed, an optimal size of the system that maximize TPES is expected. In order to investigate this effect, PEMFC size is kept equal to the actual device described in Part A, while cooling and heating loads and air flow rates are scaled up by a factor α in each time step.

At each time step, heating, cooling loads and volume flow rates are calculated, independently for AHU_{ref} and AHU_{tri}, as reported in Eqs. (15)–(17):

$$\dot{Q}_{out} = \alpha \dot{Q}_{rb,out} \tag{15}$$

$$\dot{C}_{out} = \alpha \dot{C}_{rb,out} \tag{16}$$

$$\dot{V}_a = \alpha \dot{V}_{a,rb} \tag{17}$$

In this way different air conditioning loads are compared with the same PEMFC unit and the overall TPES is evaluated. In each investigated case the ratio of PEMFC heating capacity to maximum building thermal loads is calculated through Eq. (18):

$$CR = \frac{\dot{Q}_{out,PEM,max}}{\dot{Q}_{peak,out}} = \frac{\dot{Q}_{out,PEM,max}}{\alpha \dot{Q}_{peak,rb,out}} \tag{18}$$

where $Q_{out,PEM,max}$ is the PEMFC system maximum heating capacity that, according to Part A, is equal to 52.36 kW, and $Q_{peak,rb,out}$ is the maximum load of AHU heating coils in winter time by the reference building.

5. Results and discussion

5.1. Methodology

Results are discussed in terms of seasonal and annual achievable TPES as a function of PEMFC system capacity ratio (CR) and on the most relevant design parameters.

Energy simulations are performed on hourly basis: in each step, supply air flow conditions are calculated to balance building loads. Heating and cooling processes are calculated for both air handling units and therefore, heating and cooling capacity for each heat exchanger is determined. For all locations, winter and summer periods range from 16st October to 14th April and from 15th April to 15th October respectively.

Q_{tot} and C_{tot}, which should be calculated independently for AHU_{ref} and AHU_{tri}, are defined respectively in winter and summer period in this way:

$$Q_{tot} = \sum_i Q^i_{out} = \sum_i (Q^i_{HC} + Q^i_{CC}) = \alpha \sum_i (Q^i_{rb,HC} + Q^i_{rb,CC}) \tag{19}$$

$$C_{tot} = \sum_i C^i_{out} = \sum_i C^i_{CC} = \alpha \sum_i C^i_{rb,CC} \tag{20}$$

5.2. Storage tanks size

A parametric analysis has been accomplished to assess how tank size affects the exploitation of cogenerated heat. Heat losses can be distinguished in two main components, i.e.:

- Heat losses from the tanks to the surrounding, namely $Q_{loss,LTT}$ *and* $Q_{loss,HTT}$.
- Heat rejected across the heat sinks to adjust PEMFC return water loop temperature, i.e. $Q_{loss,LTS}$ *and* $Q_{loss,HTS}$.

The former depend on tank outer surface and on the difference between tank water temperature and surrounding temperature. Therefore, the larger the tank, the higher heat losses to the surroundings. For small values of CR, that is for $\alpha >> 1$, heating loads across air handling unit heat exchangers are higher, therefore hot water is frequently drawn from heat tanks. This implies that tank average temperature over the entire operating time is lower and, in turn, thermal losses diminish.

Heat rejected across heat sinks can be significantly limited by increasing tank size: in fact, the higher the storage volume, the lower the average tank temperature and, in turn, the higher the heat released by water loop to the tank. At constant storage tank size, low values of CR implies that stored heat is rapidly exploited for air conditioning use, so heat rejection is not relevant.

Figs. 5 and 6 provide the total thermal loss fraction (tank losses and heat rejection) for different size of storage tank as a function of CR in Milan climate. The sum of total storage tank and heat sink losses, namely $Q_{loss,LT}$ *and* $Q_{loss,HT}$, are provided as percentage of total heat delivered by the fuel cell, referred to as $Q_{out,PEM}$. Heat losses are calculated as reported in Eqs. (21) and (22):

$$Q_{loss,LT} = Q_{loss,LTT} + Q_{loss,LTS} \tag{21}$$

$$Q_{loss,HT} = Q_{loss,HTT} + Q_{loss,HTT} \tag{22}$$

Energy losses due to low temperature tank are barely relevant compared to total heat provided by the PEMFC, as thermal loss fraction can drop below 2% (Fig. 5). High temperature heat is much more relevant since it represents the main PEMFC thermal output and because a high temperature difference between tank and surroundings leads to higher thermal losses (Fig. 6). In addition it is highlighted that for HTT equal to 4 m^3 heat rejection is the

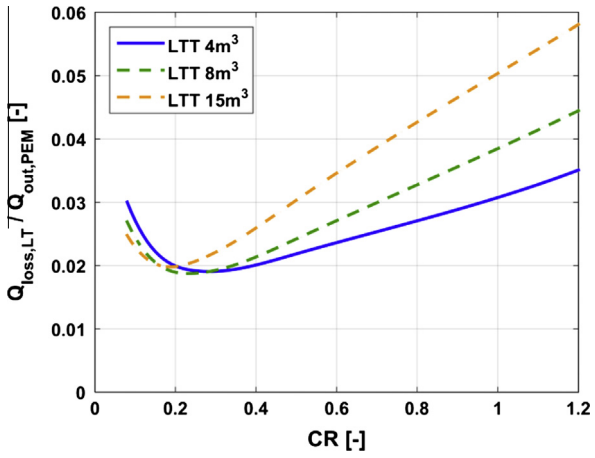

Fig. 5. Energy loss fraction as a function of CR for different size of LTT tank (HTT 8 m^3).

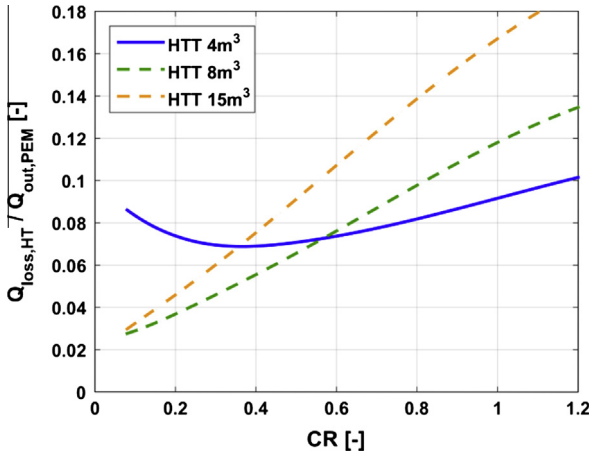

Fig. 6. Energy loss fraction as a function of CR for different size of HTT tank (LTT 4 m^3).

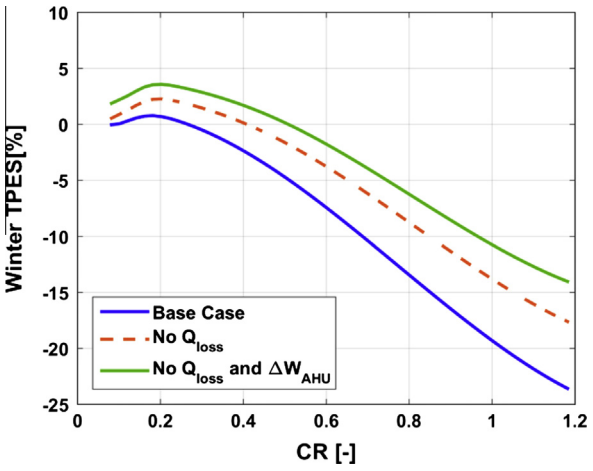

Fig. 7. Winter TPES as a function of CR (Milan).

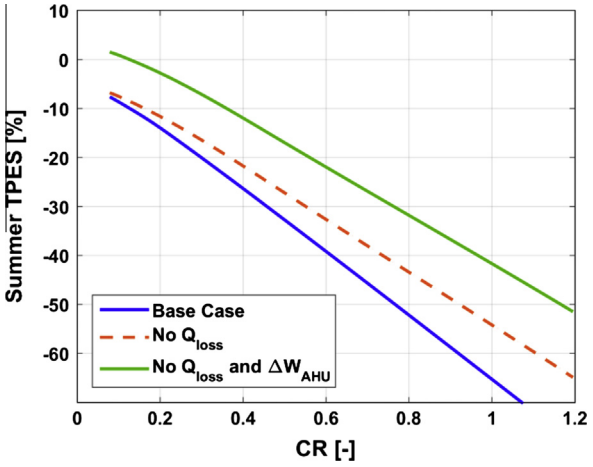

Fig. 8. Summer TPES as a function of CR (Milan).

prevalent thermal loss mechanism, especially at low values of CR. In fact if HTT is set to 4 m^3 and CR is close to 1, heat rejection energy fraction is higher than 6%, in spite of 8 m^3 or 15 m^3 scenario in which heat rejection fraction is lower than 0.5%. With large tank volumes total thermal loss almost depend on heat transfer from the tanks to the surrounding. Thermal loss fraction increases quasi-linear with CR (Fig. 6) since the PEMFC unit operates for lower time while tank average temperature is higher over the whole operating year.

According to this preliminary analysis, the following investigation will be performed with size of LTT and HTT respectively equal to 4 m^3 and 8 m^3. In addition to the information provided through Figs. 5 and 6, it is highlighted that heat sink rejection is mainly a small fraction of total thermal losses. More precisely, with the adopted tanks volumes, $Q_{loss,LTS}/Q_{loss,LT}$ is 0.9% and 0.4% respectively at CR = 0.24 and CR = 1.2. Similarly, $Q_{loss,HTS}/Q_{loss,HT}$ is 0.3% and almost zero at the same CR.

5.3. Heat losses and electrical consumption

Figs. 7 and 8 show the results of seasonal simulation in winter and summer for Milan climate. According to Fig. 7, winter primary energy saving can be slightly positive only for very low capacity ratio, with a maximum value of 0.7% for CR 0.15.

In order to understand the effect of heat losses, an additional scenario with perfect insulation of LTT and HTT is assumed (being heat rejection trough HTS and LTS almost negligible with the previously chosen tank size). If the system experiences no heat losses, maximum winter TPES rises to 2.2% for CR 0.2, which means that thermal loss to the environment reduces maximum potential TPES by 1.5%; this effect is even more remarkable for higher values of CR. Optimal value of CR slightly increases if perfect tank insulation is included in the model. This trend may be explained with a larger share of exploited cogenerated heat: no thermal losses imply a higher amount of energy stored in tanks and, in turn, a lower amount of backup boiler heat usage.

TPES is also detrimentally affected by the higher electrical consumption of the trigeneration air handling unit, being the extra consumption ΔW_{AHU} defined as in Eq. (23)

$$\Delta W_{AHU} = W_{in,tri,AHU} - W_{in,ref,AHU} \tag{23}$$

If electric consumptions of AHU_{tri} are kept equal to AHU_{ref}, i.e., the terms ΔW_{AHU} vanishes, and perfect tank insulation is still assumed, maximum winter TPES raises up to 3.6% (Fig. 7). This outlines that neglecting electrical consumption for ventilation may lead to misleading values of TPES. Moreover, this value is still far below the primary energy saving index (PES) of the same PEMFC reported by Campanari et al. [32], that is 6.07% at PEMFC full load conditions. The main reason of such a difference is that the calculation of PES considers fully exploited heat and that neglects PEMFC stand-by consumption, whose effect will be discussed in Section 5.4 of this paper.

As shown in Fig. 8, summer TPES is always negative and for very low values of CR the increase in primary energy consumption is around 7%. This is mainly due to the fact that air handling unit electricity consumption is significantly higher in summer time due to a major complexity of a DEC unit, while PEM summer electrical output is lower than winter due to a lower demand of heating in summer season.

On yearly basis, TPES is detrimentally affected by poor performance in summer, for which winter primary energy savings barely compensate. Maximum value of TPES is −2.2% for CR close to 0.08, while if no heat losses occur maximum TPES raises up to −1.2% at CR 0.16. Whether both Q_{loss} and ΔW_{AHU} are not considered, yearly TPES is positive and achieves 2.3% with optimal CR 0.16.

5.4. Effects of MSBT and stand-by consumption

In this section a sensitivity analysis on two main PEM operating parameters, namely minimum stand-by time (MSBT) and stand-by consumption, is presented. More precisely MSBT has been kept equal to 3 h in previous simulations while in the current analysis MSBT has been reduced to 1 h to assess the overall effect on system performance.

Stand-by requires the PEMFC system to be kept at proper level of temperature without delivering any useful output. In order to evaluate the effect of stand-by time on overall system performance, in the current analysis it has been assumed that the PEMFC could actually be switched off without any energy consumption ($\dot{F}_{in,PEM,SB} = 0$ kW and $\dot{W}_{in,tri,SB} = 0$ kW).

Referring to Figs. 9 and 10, it is found that MSBT is not a key parameter to optimize, since TPES remains equal as shown by the two curves that are almost overlapped. This trend may be explained thanks to storage tanks size, which have been chosen properly. Anyway it is expected that a lower MSBT can lead to a lower size of heat tanks and, therefore, to slightly lower heat losses.

Assuming zero energy consumption when PEMFC is in stand-by condition, maximum winter TPES is raised up to 3.2% with optimal CR equal to 0.25 (Fig. 9). In summer TPES still remains negative (Fig. 10) in spite of a significantly lower heating demand in summer and, in turn, a greater number of PEMFC stand-by hours. Yearly TPES is raised up from −2.2% to +0.7% and comparing with the Base Case a slight increase in optimal CR is found. This can be explained with the fact that very low values of CR increase PEMFC operating time and, on the other hand, reduce stand-by time. However, the heat delivery fraction is lower with small CR, therefore the net electrical energy yield is less relevant. Whether stand-by energy losses are negligible, TPES benefits from higher values of CR in the light of a larger heating delivery.

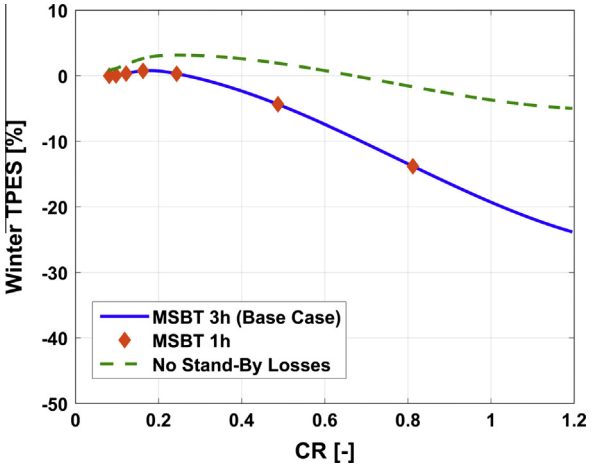

Fig. 9. Effect of MSBT and stand-by time on winter TPES (Milan).

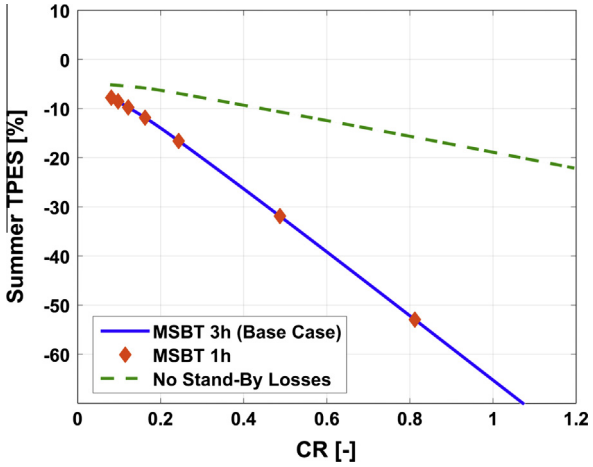

Fig. 10. Effect of MSBT and stand-by time on summer TPES (Milan).

5.5. Climate conditions

In this section annual energy simulation is performed for two other different locations, namely Freiburg and Barcelona, in order to investigate the influence of climate. These two locations differ from Milan in terms of sensible and latent loads over the year. Thermal and cooling energy requirements are provided in Table 1.

Due to a higher heating demand in winter time, the trigenerative system in Freiburg climate performs slightly better in winter time and compensate the poor performance in summer time, in which cooling demand is lower than in Milan. On yearly basis, TPES achieve a maximum value of 1.5% and −2.2% in Freiburg and Milan respectively, with an optimal value of CR close to 0.1 (Fig. 11).

The trigeneration system performs poorly in warm and humid Mediterranean climate such as Barcelona, in which heating demand is very low and total cooling is relevant (Table 1). Moreover, maximum regeneration temperature is 56.5 °C, which is significantly higher than maximum value recorded in Milan (44.4 °C). This implies that the PEMFC heat delivery is also limited by average supply temperature which is not sufficiently high to meet desiccant cooling loads, and, in turn, auxiliary boiler share can be significant even in summer.

5.6. Effects of PEMFC system improvements

The effect of potential modifications to improve PEMFC system, as discussed in part A, is provided in Fig. 12, being Modification 1 the result of air pre-heating and Modification 2 the result of air pre-heating and auxiliary devices improvement. Modification 1 is characterized by slightly higher electrical efficiency lower thermal efficiency, therefore the global effect on primary energy saving is even worse. On the other hand, Modification 2 has the same thermal efficiency of the first one but it benefits from significantly

Table 1
Annual total heating and cooling required for each location ($\alpha = 1$).

		Milan	Freiburg	Barcelona
$Q_{tot,ref}$	[MW h]	28.14	33.02	9.64
$C_{tot,ref}$	[MW h]	6.85	2.03	15.53
$Q_{tot,tri}$	[MW h]	30.11	33.14	18.24
$C_{tot,tri}$	[MW h]	4.14	1.76	7.55

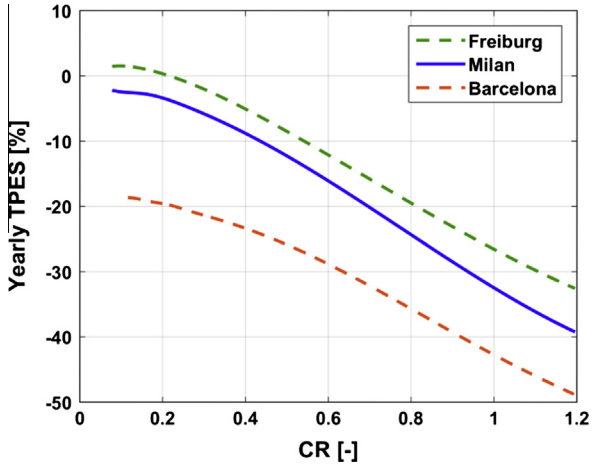

Fig. 11. Yearly TPES against as a function of CR for different locations.

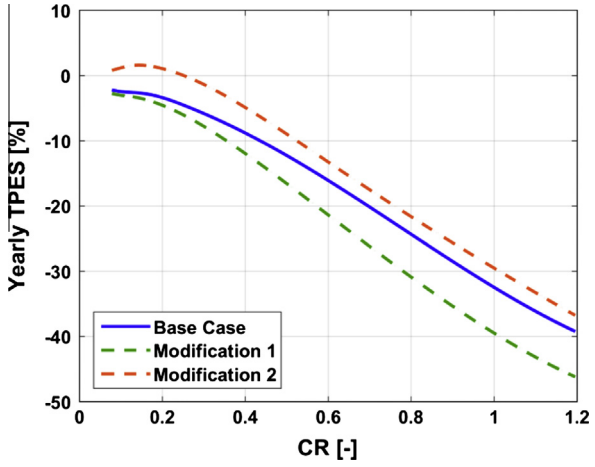

Fig. 12. Comparison of yearly TPES for base case, Modification 1 and Modification 2 (Milan).

higher values of electrical efficiency, which in turn lead to positive values of TPES on annual basis.

Based on the aforementioned considerations, the absence of stand-by losses and the improvement of PEMFC system through modification 2 can lead to promising primary energy savings: TPES would reach 5.3% when CR = 0.2. Therefore the development of future efficient systems should properly implement such technical improvements.

6. Conclusions

In the present work a trigeneration system based on PEMFC combined heat and power unit is investigated for building air conditioning. PEMFC unit is combined with a hybrid desiccant cooling system in order to exploit low temperature heat as a driver for cooling process in summer time. Such system is compared to a standard reference air conditioning system on yearly basis.

The effect of the trigenerative unit size on primary energy savings in relation to building air conditioning loads is discussed. Heat losses due to thermal coupling of the PEMFC with the air conditioning system, electrical consumption of air handling unit and PEMFC operating parameters are investigated as main sources of performance loss. A climate comparison of annual trigeneration energy saving in three different locations is also provided. Possible improvements in fuel cell efficiency are finally discussed.

It is found that heating capacity of the unit, compared to maximum air conditioning load, turns out to be a crucial design parameter in order to obtain the highest values of TPES. Optimal capacity ratio is found to be 0.15 in winter time for Milan climate conditions; limiting thermal losses raises the optimal value of CR. However, on yearly basis winter primary energy savings have to compensate for poor performance in summer time, which are detrimentally affected by high electrical consumptions and low heating and electrical energy delivered by the PEMFC. Other minor source of losses are heat losses from the storage to the environment and PEMFC stand-by which may contribute to a reduction in TPES of 1% and 3% respectively. Only limiting the electrical consumption of the trigeneration air handling unit and reducing significantly heat losses can bring to positive savings in primary energy.

It is also shown that if the climate is warmer and more humid, desiccant cooling process may be detrimental in terms of annual TPES, due to the low temperature of rejected heat from PEMFC and the resulting increase in auxiliary boiler heating. The increase in PEMFC electrical efficiency is also a crucial parameter in order to make the trigenerative system a viable alternative to up-to-date air conditioning systems. Finally, it is shown that an improvement in the PEMFC heat recovery system, in auxiliary devices efficiency and the lack of stand-by losses can increase TPES up to 5.3%, achieving significant energy savings.

Acknowledgments

Funding for this work from Italian Cassa Conguaglio Sistema Elettrico (CCSE) under agreement no. 6562 is acknowledged (project STAR— Sidera Trigenerazione Alto Rendimento).

References

[1] Kavvadias KC, Tosios AP, Maroulis ZB. Design of a combined heating, cooling and power system: operation, strategic selection and parametric analysis. Energy Convers Manage 2010;51:833–45.
[2] Balli O, Aras H, Hepbasli A. Thermodynamic and thermoeconomic analyses of a trigeneration system with a gas-diesel engine: Part I – Methodology. Energy Convers Manage 2010;51:2252–9.
[3] Balli O, Aras H, Hepbasli A. Thermodynamic and thermoeconomic analyses of a trigeneration system with a gas-diesel engine: Part II – An application. Energy Convers Manage 2010;51:2260–71.
[4] Zhao XL, Fu L, Li F, Liu H. Design and operation of a tri-generation system for a station in China. Energy Convers Manage 2014;80:391–7.
[5] Wang M, Wang J, Zhao P, Dai YP. Multi-objective optimization of a combined cooling, heating and power system driven by solar energy. Energy Convers Manage 2015;89:289–97.
[6] Al-Sulaiman FA, Dincer I, Hamdullahpur F. Thermoeconomic optimization of three trigeneration systems using organic Rankine cycles: Part II – Applications. Energy Convers Manage 2013;69:209–16.
[7] Sonar D, Soni SL, Sharma D. Micro-trigeneration for energy sustainability: technologies, tools and trends. Appl Therm Eng 2014;71:790–6.
[8] Elmer T, Worall M, Wu S, Riffat SB. Fuel cell technology for domestic built environment applications: state of-the-art review. Renew Sust Energy Rev 2015;42:913–31.
[9] Gluesenkamp K, Hwang Y, Radermacher R. High efficiency trigeneration systems. Appl Therm Eng 2013;50:1480–6.
[10] Gabbar HA, Runge J, Bondarenko D, Bower L, Pandya D, Musharavati F, et al. Performance evaluation of gas-power strategies for building energy conservation. Energy Convers Manage 2015;93:187–96.
[11] Choudhury A, Chandra H, Arora A. Application of solid oxide fuel cell technology for power generation – a review. Renew Sust Energy Rev 2013;20:430–42.
[12] Zink F, Lu Y, Schaefer L. A solid oxide fuel cell system for buildings. Energy Convers Manage 2007;48:809–18.
[13] Chen JMP, Ni M. Economic analysis of a sold oxide fuel cell cogeneration/trigeneration system for hotels in Hong Kong. Energy Build 2014;75:160–9.
[14] Ranjbar F, Chitsaz A, Mahmoudi SMM, Khalilarya S, Rosen MA. Energy and exergy assessment of a novel trigeneration system based on solid oxide fuel cell. Energy Convers Manage 2014;87:318–27.
[15] Fong KF, Lee CK. Investigation on zero grid-electricity design strategies of solid oxide fuel cell trigeneration system for high-rise building in hot and humid climate. Appl Energy 2014;114:426–33.

[16] Al-Sulaiman FA, Dincer I, Hamdullahpur F. Energy analysis of a trigeneration plant based on solid oxide fuel cell and organic Rankine cycle. Int J Hydrogen Energy 2010;35:5104–13.
[17] Tse LKC, Wilkins S, McGlashan N, Urban B, Martinez-Botas R. Solid oxide fuel cell/gas turbine trigeneration system for marine applications. J Power Sources 2011;196:3149–62.
[18] Arsalis A, Nielsen MP, Kær SK. Modelling and off-design of a 1 kW_e HT-PEMFC-based residential micro-CHP system for Danish single family households. Energy 2011;36:993–1002.
[19] Vadiee A, Yaghoubi M, Sardella M, Farjam P. Energy analysis of fuel cell system for commercial greenhouse application – a feasibility study. Energy Convers Manage 2015;89:925–32.
[20] Najafi B, Mamaghani AH, Baricci A, Rinaldi F, Casalegno A. Mathematical modelling and parametric study on a 30 kW_{el} high temperature PEM fuel cell based residential micro cogeneration plant. Int J Hydrogen Energy 2015;40:1569–83.
[21] Jannelli E, Minutillo M, Perna A. Analyzing microcogeneration systems based on LT-PEMFC and HT-PEMFC by energy balances. Appl Energy 2013;108: 82–91.
[22] Ratlamwala TAH, Gadalla MA, Dincer I. Performance assessment of a combined PEM fuel cell and triple-effect absorption cooling system for cogeneration applications. Fuel Cells 2011;3:413–23.
[23] Ortiga J, Marimon MA, Bruno JC, Lopez E, Coronas A. Integration of new small scale sorption chillers with a PEM fuel cell of 5 kW. HYCELTEC Bilbao; 2008.
[24] Henning H-M, Pagano T, Mola S, Wiemken E. Micro tri-generation system for indoor air conditioning in the Mediterranean climate. Appl Therm Eng 2007; 27:2188–94.
[25] Myat A, Choon NK, Thu K, Kim T-D. Experimental investigation on the optimal performance of Zeolite–water adsorption chiller. Appl Energy 2013;102: 582–90.
[26] Kim DS, Infante Ferreira CA. Air-cooled LiBr–water absorption chillers for solar air conditioning in extremely hot weathers. Energy Convers Manage 2009;50: 1018–25.
[27] Angrisani G, Minichiello F, Rosselli C, Sasso M. Desiccant HVAC system driven by a micro-CHP: experimental analysis. Energy Build 2010;42:2028–35.
[28] Angrisani G, Rosselli C, Sasso M, Tariello F. Dynamic performance assessment of a micro-trigeneration system with a desiccant-based air handling unit in Southern Italy climatic conditions. Energy Convers Manage 2014;80:188–201.
[29] Zhang LZ, Niu JL. A pre-cooling Munters environmental control desiccant cooling cycle in combination with chilled-ceiling panels. Energy 2003;28:275–92.
[30] Hao X, Zhang G, Chen Y, Zou S, Moschandreas DJ. A combined system of chilled ceiling, displacement ventilation and desiccant dehumidification. Build Environ 2007;42:3298–308.
[31] Chicco G, Mancarella P. Trigeneration primary energy saving for energy planning and policy development. Energy Policy 2007;35:6132–44.
[32] Campanari S, Valenti G, Macchi E, Lozza G, Ravidà N. Development of a micro-cogeneration laboratory and testing of a natural gas CHP unit based on PEM fuel cells. Appl Therm Eng 2013;71:714–20.
[33] Pennington NA. Humidity changer for air conditioning. US Patent 2, 700,537.
[34] AERMEC. Vapour compression chiller technical data sheet; 2015. Retrieved from <http://www.aermec.com/> [visited on 08.07.15].
[35] Duffie J, Beckman W. Solar engineering of thermal processes. 4th ed. Hoboken, New Jersey: John Wiley and Sons, Inc; 2013. p. 373–84.
[36] Fanney AH, Dougherty BP. Thermal performance of residential electric water heaters subjected to various off-peak schedules. J Sol Energ- T Asme 1996;118:73–80.
[37] SitalKlima Catalogue; 2015. Retrieved from <http://www.sitalklima.it/> [visited on 15.01.15].
[38] De Antonellis S, Joppolo CM, Molinaroli L. Simulation, performance analysis and optimization of desiccant wheels. Energy Build 2010;42:1386–93.
[39] De Antonellis S, Intini M, Joppolo CM, Leone C. Design optimization of heat wheels for energy recovery in HVAC systems. Energies 2014;7:7348–67.
[40] Henning HM. In: Solar-assisted air-conditioning in buildings – a handbook for planners. Wien: Springer Wien New York; 2007. p. 90–1.
[41] Najafi B, De Antonellis S, Intini M, Zago M, Rinaldi F, Casalegno A. A tri-generation system based on polymer electrolyte fuel cell and desiccant wheel – Part A: Fuel cell system modelling and partial load analysis. Energy Convers Manage 2015. http://dx.doi.org/10.1016/j.enconman.2015.10.004.